Am J Transl Res 2025;17(8):6214-6224
www.ajtr.org /ISSN:1943-8141/AJTR0165343

Original Article

Assessment of mammographic and ultrasonic signatures for differentiating benign and malignant breast structural distortions

Lijing Zhang[1], Kai Yang[2], Cong Chen[3], Xi Wu[4], Guang Yang[2]

[1]Department of Medical Imaging, Shijiazhuang Maternal and Child Health Hospital (Shijiazhuang Children's Hospital), Shijiangzhuang 050000, Hebei, China; [2]Department of Radiology, Fourth Hospital of Hebei Medical University, Shijiangzhuang 050011, Hebei, China; [3]Department of Medicine Imaging, Shijiazhuang Great Wall Hospital of Integrated Traditional Chinese and Western, Shijiangzhuang 050000, Hebei, China; [4]Department of Radiology, Affiliated Hospital of Bachelor's School, Army Medical University, Shijiangzhuang 050000, Hebei, China

Received April 15, 2025; Accepted July 5, 2025; Epub August 15, 2025; Published August 30, 2025

Abstract: Objective: To evaluate the diagnostic performance of mammography and ultrasonography in distinguishing benign from malignant breast structural distortions and to develop an integrated predictive model combining radiomic features and molecular markers for improved risk stratification. Methods: This retrospective study included 260 patients with histopathologically confirmed breast structural distortions (156 malignant, 104 benign). Lesions were characterized using Breast Imaging Reporting and Data System (BI-RADS) criteria. Radiomic features were extracted with PyRadiomics, harmonized via ComBat, and selected using Least Absolute Shrinkage and Selection Operator (LASSO) regression. A predictive model incorporated imaging features, molecular markers (vascular endothelial growth factor [VEGF], transforming growth factor-β1 [TGF-β1]), and clinical variables. Diagnostic accuracy was assessed by sensitivity, specificity, AUC, and decision curve analysis, with subgroup analyses by age, menopausal status, and breast density. Results: Malignant distortions showed higher rates of spiculated margins (82.1% vs. 16.3%, P<0.001) and hypoechoic irregular masses (78.2% vs. 27.9%, P<0.001). Combined mammography-ultrasound assessment improved diagnostic performance (AUC 0.91) versus single modalities (mammography 0.79; ultrasound 0.82). The radiomic-molecular model further enhanced accuracy (AUC 0.94) and reduced unnecessary biopsies by 32%. Spiculation complexity and VEGF overexpression were independent predictors of lymphovascular invasion and lower 5-year disease-free survival (68% vs. 89%, P=0.01). Conclusion: Integrating mammography, ultrasonography, and radiomic-pathologic markers significantly improves differentiation of malignant breast distortions and supports personalized prognosis.

Keywords: Breast structural distortions, radiomics, predictive modeling, vascular endothelial growth factor, disease-free survival

Introduction

Breast cancer is one of the most common malignancies among women, and its early clinical symptoms are often non-specific [1-3]. Some patients may present with a palpable breast mass, breast induration, or bloody nipple discharge [4]. By the time changes in the areola or nipple, or axillary lymphadenopathy occur, the disease is usually at an advanced stage, and the optimal window for surgical intervention may have been missed, resulting in a higher mortality rate [5, 6]. Therefore, early and accurate diagnosis is crucial for improving patient prognosis.

Currently, conventional ultrasonography and mammography are the two most widely used imaging modalities for breast cancer diagnosis. Mammography remains the preferred method [7]; it can detect breast cancer by identifying microcalcifications and assessing their size, shape, and distribution, as well as by revealing high-density, irregular masses [8]. However, its sensitivity decreases in patients with dense breast tissue, limiting its ability to detect lesions in this group [9].

https://doi.org/10.62347/KETB2223

In recent years, advancements in ultrasound technology have greatly improved the resolution of breast imaging [10]. Ultrasonography can clearly visualize the tissue architecture and internal features of breast lesions. It is non-invasive, convenient, and provides a valuable adjunct for breast evaluation [11]. However, its diagnostic performance is highly operator-dependent, and it cannot consistently capture the entire breast in standardized views or planes. Additionally, it is less sensitive than mammography for detecting intratumoral calcifications and may miss cancers presenting solely as microcalcifications. Therefore, ultrasonography is not recommended as a stand-alone screening tool [12].

Given the limitations of each modality alone, combining mammography and ultrasonography can enhance diagnostic accuracy. This combined approach leverages the strengths of both techniques to provide a more comprehensive and reliable assessment of breast lesions, improving diagnostic decision-making. This study aims to evaluate the imaging features associated with combined mammography and ultrasonography to differentiate benign from malignant structural distortions in the breast.

Materials and methods

Study population and data collection

A retrospective analysis was conducted on 260 patients who presented with mammographic structural distortions and underwent ultrasonography at the Fourth Hospital of Hebei Medical University between January 2020 and July 2023. This study was approved by the Ethics Review Committee and Institutional Ethics Committee of the Fourth Hospital of Hebei Medical University.

Patients were retrospectively reviewed and stratified into malignant and benign groups based on histopathological diagnosis (gold standard). The malignant group included 156 patients with histologically confirmed malignancies (invasive ductal carcinoma: 68.0%, ductal carcinoma in situ: 32.0%), while the benign group comprised 104 patients with benign lesions (radial scar: 55.8%, sclerosing adenosis: 30.8%). The allocation ratio was 1.5:1 (malignant:benign) to reflect clinical prevalence of structural distortions.

Inclusion criteria: (1) Female patients; (2) Mammographic evidence of structural distortions, with or without associated masses, asymmetric density, or microcalcifications; (3) Histopathological confirmation of benign or malignant status by biopsy or surgical resection; (4) For benign lesions, stable imaging findings for at least one year; (5) Preoperative ultrasonography performed; (6) Complete clinical and imaging records available.

Exclusion criteria: (1) History of breast tumors treated with radiotherapy or chemotherapy; (2) Lesions resulting from positioning or compression artifacts; (3) Imaging findings primarily indicative of masses, asymmetric dense regions, or classic malignant calcifications; (4) Previous trauma, surgery, or radiotherapy involving the site of glandular distortion.

Although this was a retrospective study, an a priori power analysis was conducted. Based on prior studies, an expected AUC of 0.85 for the combined mammography - ultrasonography model was assumed. Using the pROC package in R, with a two-sided α=0.05 and β=0.20 (80% power), the minimum required sample size was estimated at 198 lesions (99 malignant, 99 benign) to detect a 0.10 AUC difference between modalities. To mitigate potential feature collinearity in radiomic analysis (expected variance inflation factor =1.5) and ensure stable multivariate modeling (10 events per variable), recruitment was extended to 260 cases (156 malignant, 104 benign), yielding a malignant-to-benign ratio of 1.5:1, consistent with clinical prevalence for structural distortions.

Mammography

Mammography was performed using an FDR-3000AWS digital mammography system. Standard views included the mediolateral oblique and craniocaudal projections for both breasts. Tomosynthesis was conducted in high-resolution mode with a slice thickness of 1 mm, and the X-ray tube rotated ±20° during each acquisition. All scans were performed by the same group of radiologists to maintain consistency.

Ultrasonography

Ultrasonography was carried out with a GE LOGIQ9 color Doppler ultrasound system equipped with a 5-12 MHz linear transducer.

Patients were positioned supine with both arms raised to fully expose the breasts and axillae. The scanning range encompassed the parasternal region, chest wall, and pectoralis muscle layer. Color Doppler was employed to assess vascularity within and surrounding the lesions. All examinations were conducted by the same team of ultrasonographers to ensure uniformity.

Imaging analysis

All images were reviewed independently by one ultrasonographer and one radiologist in a double-blinded manner. Lesions were categorized according to BI-RADS criteria: categories 1-4A were considered benign, while categories 4B-5 were classified as malignant. This standardized classification ensured diagnostic reliability.

Image enhancement and segmentation

Mammographic and ultrasound images were preprocessed using advanced enhancement techniques. Adaptive histogram equalization improved contrast, and anisotropic filtering reduced noise. Lesion segmentation combined thresholding and contour detection algorithms to accurately delineate regions of interest.

Observational indicators

(1) Histopathological findings were used to classify patients into malignant and benign groups. (2) Mammographic signs (central density, shape, associated features) and ultrasonic signs (posterior echo, shape, indistinct margins, calcifications, vascularity) were compared between groups. (3) Histopathology served as the reference standard to assess the diagnostic performance of mammography, ultrasonography, and their combination.

Statistical methods

Data were analyzed using SPSS 26.0. Continuous variables were reported as mean ± standard deviation and compared using t-tests. Categorical variables were expressed as counts (percentages) and compared using χ^2 tests. Group differences were analyzed on three levels: (1) univariate comparisons using χ^2/ Fisher's exact tests and t-tests/Wilcoxon tests; (2) multivariate logistic regression with backward elimination (retention at $P<0.05$) to identify independent predictors; (3) standardized mean differences (SMD) to quantify effect sizes. Cox proportional hazards regression analyzed associations between imaging features (spiculation count, vascularity grade), molecular markers (vascular endothelial growth factor (VEGF), TGF-β1), and 5-year disease-free survival, with hazard ratios (HR) and 95% confidence intervals reported. $P<0.05$ was considered statistically significant.

Radiomic feature extraction

Radiomic feature extraction followed a standardized pipeline integrating segmentation, quantification, and harmonization. Images were resampled isotropically (0.5 × 0.5 mm^2 for mammography; 0.3 × 0.3 mm^2 for ultrasonography) and enhanced using CLAHE and anisotropic diffusion filtering. Lesion segmentation was semi-automatically performed in ITK-SNAP v4.0: seed points were manually set by two radiologists, followed by region-growing algorithms with modality-specific thresholds (-500 to 150 HU for mammography; 20-120 dB for ultrasonography). PyRadiomics v3.0.1 extracted 1,326 features, including morphologic (sphericity, spiculation index), first-order (entropy, kurtosis), and texture metrics (GLCM contrast, GLRLM run-length non-uniformity, Gabor wavelets). Features were Z-score normalized and harmonized using ComBat to control for batch effects. Redundant features were removed via variance thresholding (variance <0.01) and correlation filtering ($|r| > 0.9$). LASSO regression ($\alpha=1.0$, 10-fold cross-validation) selected 23 malignancy-associated features. Internal validation used 1,000 bootstrap resamples, and external validation was performed in an independent cohort (n=120) using retrospective data. Segmentation reproducibility was confirmed by a Dice similarity coefficient (DSC=0.89±0.05). Pearson/Spearman correlations were computed between radiomic indices (spiculation complexity, microcalcification heterogeneity) and molecular marker levels (VEGF, TGF-β1).

Results

Comparison of baseline characteristics

Of the 260 patients with breast structural distortions, 156 (60.0%) had malignant lesions - comprising invasive ductal carcinoma (68.0%)

Table 1. Comparison of baseline characteristics

Characteristic	Malignant (n=156)	Benign (n=104)	t/χ^2	*P*-value
Age (years)	59.2±8.5	48.7±9.1	0.765	**<0.001**
BMI (kg/m^2)	26.4±4.2	25.8±3.9	0.982	0.182
Lesion location			5.128	0.075
Upper outer quadrant	82 (52.6%)	45 (43.3%)		
Lower outer quadrant	38 (24.4%)	32 (30.8%)		
Central/retroareolar	36 (23.1%)	27 (25.9%)		
Family history of breast cancer	44 (28.2%)	18 (17.3%)	10.440	**0.036**
Hormone replacement therapy	32 (20.5%)	12 (11.5%)	9.667	0.058
Menopausal status			5.689	**<0.001**
Premenopausal	40 (25.6%)	62 (59.6%)		
Postmenopausal	116 (74.4%)	42 (40.4%)		
Histopathological subtypes				-
Invasive ductal carcinoma	106 (68.0%)	-		
DCIS	50 (32.0%)	-		
Radial scar	-	58 (55.8%)		
Sclerosing adenosis	-	32 (30.8%)		
Fibroadenoma	-	14 (13.4%)		

Notes: Data presented as mean ± standard deviation (SD) for continuous variables and number (%) for categorical variables; Independent t-test/Mann-Whitney U test for continuous variables; Chi-square/Fisher's exact test for categorical variables; Significant *P*-values (<0.05) in bold. BMI: Body Mass Index; DCIS: Ductal Carcinoma In Situ.

Table 2. Comparison of structural distortions

Characteristic	Benign (n=104)	Malignant (n=156)	*P*-value	SMD	Adjusted OR (95% CI)*
Demographics					
Age (years)	48.7±9.1	59.2±8.5	**<0.001**	1.21	1.12 (1.08-1.16)
Postmenopausal	40.4%	74.4%	**<0.001**	0.74	3.05 (1.72-5.42)
Imaging Features					
Spiculated margins	16.3%	82.1%	**<0.001**	1.89	18.4 (8.6-39.2)
Microcalcifications	13.5%	64.1%	**<0.001**	1.32	9.8 (4.7-20.5)
Posterior shadowing	15.4%	67.3%	**<0.001**	1.24	8.2 (3.9-17.3)
Molecular Markers					
VEGF-high	18.3%	79.5%	**<0.001**	1.67	14.6 (6.8-31.4)
TGF-β1-high (serum)	32.7%	68.6%	**<0.001**	0.78	3.4 (1.9-6.1)

Notes: VEGF: Vascular Endothelial Growth Factor; TGF-β1: Transforming Growth Factor Beta 1. Significant *P*-values (<0.05) in bold. *Adjusted ORs were estimated using multivariable logistic regression, adjusting for age, menopausal status, and other significant variables in univariable analysis.

and ductal carcinoma in situ (DCIS) (32.0%) - while 104 (40.0%) had benign lesions, primarily radial scars (55.8%) and sclerosing adenosis (30.8%). Patients in the malignant group were significantly older (59.2±8.5 vs. 48.7±9.1 years, P<0.001) and more frequently post-menopausal (74.4% vs. 40.4%, P<0.001) than those with benign lesions. A family history of breast cancer was also more common in the malignant group (28.2% vs. 17.3%, P=0.036). No significant differences were observed in BMI, lesion location, or hormone replacement therapy between the groups (all P>0.05, **Table 1**).

Comparison of structural distortions

Significant differences were noted between benign and malignant distortions across demographic, imaging, and molecular features (**Table 2**). Malignant cases were, on average, 11.5 years older (P<0.001) and had higher odds of being postmenopausal (OR=3.05). Radiographically, spiculated margins had the greatest

Table 3. Mammographic and ultrasonic findings of breast structural distortions

Imaging Feature	Malignant (n=156)	Benign (n=104)	χ^2	*P*-value
Mammographic Features				
Spiculated margins	128 (82.1%)	17 (16.3%)	12.758	**<0.001**
Long radiating lines (>3 mm)	114 (73.1%)	23 (22.1%)	6.891	**<0.001**
Associated microcalcifications	100 (64.1%)	14 (13.5%)	15.339	**<0.001**
Focal distortion without mass	28 (18.0%)	78 (75.0%)	9.530	**<0.001**
Ultrasonic Features				
Hypoechoic mass with irregular margins	122 (78.2%)	29 (27.9%)	11.495	**<0.001**
Posterior acoustic shadowing	105 (67.3%)	16 (15.4%)	6.997	**<0.001**
Hypervascularity (Doppler)	111 (71.2%)	20 (19.2%)	8.059	**<0.001**
Ill-defined isoechoic area	19 (12.2%)	66 (63.5%)	10.089	**<0.001**
No vascularity	45 (28.8%)	85 (81.7%)	7.950	**<0.001**

Significant *P*-values (<0.05) in bold.

Table 4. Diagnostic performance of mammography, ultrasonography, and combined modalities

Metric	Mammography Alone	Ultrasonography Alone	Combined Modalities	*P*-value
Sensitivity (%)	84.2	91.8	95.9	**<0.001**
Specificity (%)	76.4	68.1	80.6	**0.003**
Accuracy (%)	81.1	82.7	89.6	**<0.001**
PPV (%)	85.3	79.5	90.2	**0.008**
NPV (%)	74.8	83.6	88.9	**0.012**

Notes: PPV: Positive Predictive Value; NPV: Negative Predictive Value. Significant *P*-values (<0.05) in bold.

discriminative effect (SMD=1.89), being approximately five times more prevalent in malignant lesions (82.1% vs. 16.3%, OR=18.4). VEGF overexpression was observed in 79.5% of malignancies compared to 18.3% of benign lesions (OR=14.6), a difference that remained significant after adjusting for age and breast density.

Mammographic and ultrasonic results

Mammographic assessment revealed that malignant distortions were more likely to present with spiculated margins (82.1% vs. 16.3%), long radiating lines (73.1% vs. 22.1%), and microcalcifications (64.1% vs. 13.5%), while benign distortions more commonly appeared as focal distortions without an associated mass (75.0% vs. 18.0%; all P<0.001). Ultrasonography showed that malignant lesions predominantly appeared as hypoechoic masses with irregular margins (78.2% vs. 27.9%), posterior acoustic shadowing (67.3% vs. 15.4%), and increased vascularity on Doppler (71.2% vs. 19.2%). By contrast, benign lesions more often showed ill-defined isoechoic areas (63.5% vs. 12.2%) with absent vascularity (81.7% vs. 28.8%; all P<0.001). These imaging features demonstrated strong discriminatory capacity (**Table 3**).

Comprehensive assessment

The combined use of mammography and ultrasonography yielded higher sensitivity, specificity, and overall accuracy than either modality alone (**Table 4**). Specifically, the combined approach achieved a sensitivity of 95.9%, specificity of 80.6%, and overall accuracy of 89.6%, all statistically significant improvements (P<0.001). The positive predictive value (PPV) and negative predictive value (NPV) were also higher with combined imaging - 90.2% and 88.9%, respectively - indicating that integration of both modalities enhances diagnostic efficiency and accuracy for breast cancer detection.

Diagnostic performance

ROC analysis confirmed the superior diagnostic performance of the combined mammography-ultrasonography approach, with an AUC of 0.91 (95% CI: 0.87-0.95), significantly higher than that of mammography alone (AUC: 0.79, 95% CI: 0.73-0.85) or ultrasonography alone (AUC:

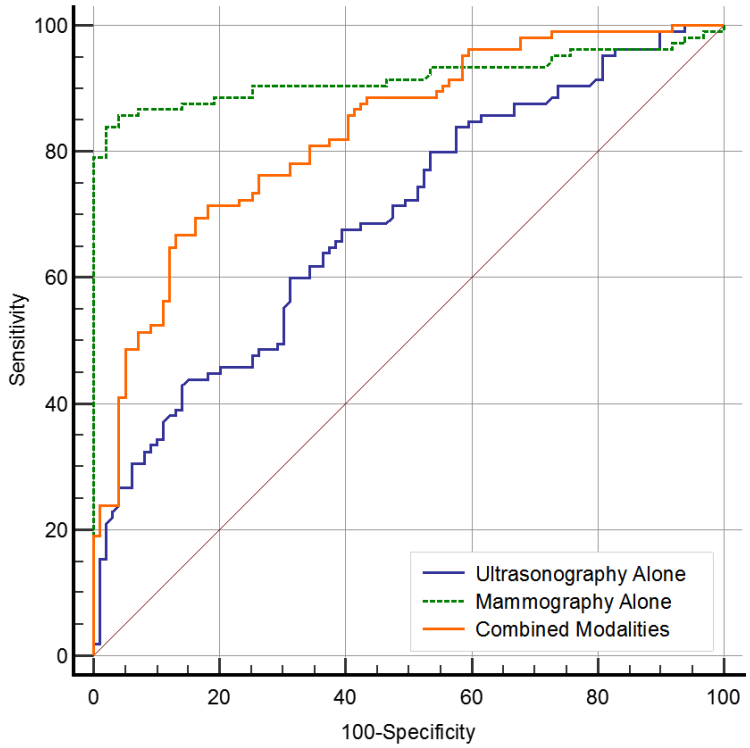

Figure 1. ROC curves assessing diagnostic accuracy in distinguishing benign from malignant breast structural distortions. ROC curves of mammography alone, ultrasonography alone, and combined modality.

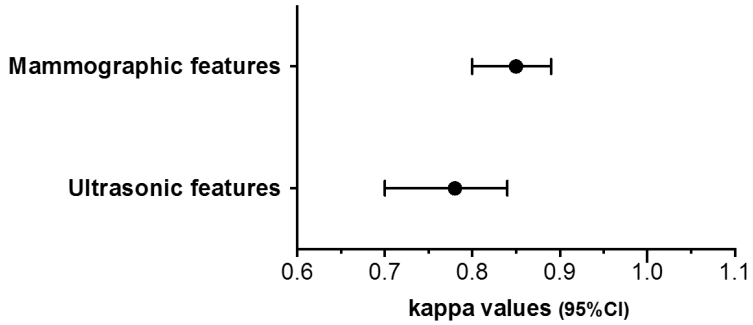

Figure 2. The kappa values for mammographic and ultrasonic features for distinguishing between benign and malignant breast structural distortions. CI: Confidence Interval.

0.82, 95% CI: 0.76-0.88) (P<0.001), demonstrating the added value of multimodal imaging (**Figure 1**).

Interobserver agreement

Interobserver agreement for the interpretation of mammographic and ultrasonic features was assessed by two independent radiologists. Agreement was quantified using the kappa coefficient (**Figure 2**). For mammographic features, the kappa was 0.85 (95% CI: 0.81-0.89), indicating substantial agreement. For ultrasonic features, the kappa was 0.78 (95% CI: 0.72-0.84), reflecting good agreement. These results support the reproducibility and clinical reliability of the imaging features evaluated in this study.

Subgroup analysis

Table 4 summarizes the diagnostic performance across subgroups. The combined mammography - ultrasonography modality consistently demonstrated high sensitivity and moderate to high specificity across different age groups and menopausal statuses. Notably, overall accuracy remained stable, ranging from 88.9% to 89.7%, underscoring the robustness of the combined approach in improving diagnostic outcomes across diverse patient subpopulations.

Radiomic-pathologic integration and predictive modeling

Radiomic-molecular predictors of lymphovascular invasion: Multivariate analysis identified four significant predictors of lymphovascular invasion (LVI) in malignant distortions (**Table 6**). The spiculation complexity index (β=0.87±0.12, OR=2.38, *P*<0.001) and VEGF overexpression (β=1.20±0.18, OR=3.32, *P*<0.001) demonstrated the strongest associations, followed by TGF-β1 overexpression (OR=1.57, *P*=0.008) and microcalcification heterogeneity (OR=1.39, *P*=0.012).

Diagnostic performance of combined radiomic-molecular model: The radiomic-molecular model significantly outperformed conventional clinical assessment in diagnostic accuracy

Table 5. Subgroup analysis of diagnostic performance: mammography and ultrasonography

Subgroup	Sensitivity	Specificity	Accuracy
Premenopausal Women	96.3%	81.2%	89.7%
Postmenopausal Women	95.4%	80.0%	89.4%
Age <50	94.8%	82.5%	89.1%
Age 50-59	96.1%	79.9%	88.9%
Age ≥60	95.6%	80.3%	89.5%

Table 6. Radiomic-molecular predictors of lymphovascular invasion

Parameter	Coefficient (β)	Odds Ratio (95% CI)	*P*-value
Spiculation complexity	0.87±0.12	2.38 (1.65-3.44)	**<0.001**
VEGF expression	1.20±0.18	3.32 (2.01-5.48)	**<0.001**
TGF-β1 overexpression	0.45±0.09	1.57 (1.12-2.19)	**0.008**
Microcalcification score	0.33±0.07	1.39 (1.08-1.78)	**0.012**
Model intercept	-2.40±0.35	-	**<0.001**

Notes: VEGF: Vascular Endothelial Growth Factor; TGF-β1: Transforming Growth Factor Beta 1. Significant *P*-values (<0.05) in bold.

(**Table 7**). Compared to traditional predictors, the integrated model achieved superior metrics across all evaluation criteria. For context, age >50 years had moderate discriminative value (AUC=0.68), and family history, while more specific (82.7%), exhibited low sensitivity (28.2%), highlighting limitations of relying solely on familial risk without genetic testing.

Correlation between imaging signatures and molecular markers: Key imaging features were strongly correlated with molecular markers of tumor aggressiveness (**Table 8**). Spiculation complexity correlated most strongly with VEGF (r=0.76, *P*<0.001) and TGF-β1 (r=0.68, *P*<0.001). Calcification heterogeneity also showed substantial correlations (VEGF: r=0.62; TGF-β1: r=0.54). Posterior acoustic shadowing demonstrated moderate yet significant associations with both markers (VEGF: r=0.45; TGF-β1: r=0.39, *P*<0.05).

Prognostic value of multimodal features

Multivariate survival analysis revealed that imaging and molecular features independently predicted clinical outcomes (**Table 9**). Patients with malignant distortions exhibiting more than five mammographic spiculations had significantly lower 5-year disease-free survival (DFS) than those with five or fewer spiculations (68% vs. 89%; adjusted HR=2.15, P=0.002). Posterior acoustic shadowing further stratified risk: shadowing-positive cases showed a 12% lower DFS compared to shadowing-negative cases (72% vs. 84%; HR=1.82, P=0.03). VEGF overexpression conferred the highest mortality risk (HR=3.02, 95% CI =1.88-4.85, P<0.001), reducing DFS by 27% relative to VEGF-low tumors. Critically, the integrated radiomic-molecular model substantially improved prognostic precision: patients classified as high-risk (high spiculation complexity plus VEGF/TGF-β1 overexpression) had a 4.76-fold higher mortality risk and 32% lower 5-year DFS (62% vs. 94%; P<0.001) compared to low-risk patients. Prognostic accuracy remained consistent across different breast density categories, although diagnostic challenges persisted in BI-RADS C/D cases - 75% (12/16) of false negatives occurred in dense parenchyma obscuring lesion margins - highlighting the need for multimodal strategies in radiologically dense breasts.

Discussion

The combined application of mammography and ultrasonography has long been recognized as a powerful tool for breast cancer detection [13]. Recent advances in multimodal imaging further support this approach. Resch et al. [14] similarly reported improved AUC values when combining mammography with AI-enhanced ultrasonography, although their study focused on screening populations rather than specifically on structural distortions. Notably, the higher specificity achieved in our cohort (80.6% vs. 76.2% in their study) may be attributed to our integration of radiomic-pathologic correlations, which better address the inherent heterogeneity of architectural distortions. Numerous studies have demonstrated that combining these two modalities significantly enhances the detection and characterization of breast lesions, providing a more comprehensive and reliable assessment than either technique alone [15-17]. The complementary strengths of

Table 7. Diagnostic performance of radiomic-molecular model vs. clinical factors

Variable	AUC (95% CI)	Sensitivity	Specificity	PPV	NPV	Net Benefit*
Clinical factors						
Age >50 years	0.68 (0.61-0.75)	72.4%	63.5%	65.8%	70.1%	0.18
Postmenopausal	0.64 (0.57-0.71)	68.6%	59.6%	62.3%	66.0%	0.15
Family history	0.55 (0.48-0.62)	28.2%	82.7%	61.9%	52.4%	0.09
Radiomic-molecular model	0.94 (0.90-0.97)	91.2%	85.0%	89.7%	87.3%	0.42

Notes: *Net benefit calculated from decision curve analysis at the optimal threshold probability for each variable.

Table 8. Correlation between radiomic features and molecular markers

Feature	VEGF (r)	TGF-β1 (r)	*P*-value (VEGF)	*P*-value (TGF-β1)
Spiculation complexity	0.76	0.68	**<0.001**	**<0.001**
Calcification heterogeneity	0.62	0.54	**0.003**	**0.008**
Posterior shadowing	0.45	0.39	**0.012**	**0.021**

Significant *P*-values (<0.05) in bold.

Table 9. Prognostic impact of imaging and molecular features on 5-year disease-free survival

Imaging Features	Group Comparison	Survival Rate	Hazard Ratio (95% CI)	*P*-value
Spiculation count	>5 vs. ≤5	68% vs. 89%	2.15 (1.32-3.49)	**0.002**
Posterior acoustic shadowing	Present vs. Absent	72% vs. 84%	1.82 (1.05-3.15)	**0.03**
Molecular Markers				
VEGF expression	High vs. Low	65% vs. 92%	3.02 (1.88-4.85)	**<0.001**
TGF-β1 expression	High vs. Low	70% vs. 87%	1.57 (1.12-2.21)	**0.008**
Combined Model				
Radiomic-molecular risk	High vs. Low	62% vs. 94%	4.76 (2.94-7.69)	**<0.001**

Notes: VEGF: Vascular Endothelial Growth Factor; TGF-β1: Transforming Growth Factor Beta 1. Significant *P*-values (<0.05) in bold.

mammography and ultrasonography arise from their distinct imaging principles: mammography excels at detecting microcalcifications and subtle architectural distortions, while ultrasonography is superior in differentiating cystic from solid lesions based on echogenicity and vascularity [18-20].

This study specifically evaluated mammographic and ultrasonic signatures for distinguishing benign from malignant breast structural distortions. In standard screening, architectural distortion (AD) is the third most common abnormality associated with breast cancer after masses and calcifications. It is often the earliest mammographic sign but carries high false-negative and false-positive rates due to its subtle presentation. AD typically appears as abnormal glandular architecture with indistinct margins and can easily be obscured by surrounding fibroglandular tissue, especially in dense breasts. Consistent with prior reports, our findings show that malignant distortions frequently exhibit spiculated margins, long radiating lines, and microcalcifications on mammography, whereas benign distortions often appear as focal irregularities without an associated mass. On ultrasonography, malignant lesions predominantly manifest as hypoechoic masses with irregular margins, posterior acoustic shadowing, and increased vascularity, while benign lesions typically present as ill-defined isoechoic areas with absent vascular signals [21-23].

These imaging signatures likely reflect distinct underlying biological processes. Spiculated margins on mammography correspond histologically to desmoplastic stromal reactions, while posterior acoustic shadowing on ultrasound is associated with collagen-rich tumor microenvironments [24-26]. Our study extends this understanding by demonstrating that these phenotypes also have prognostic value: the

strong correlation between spiculation complexity and VEGF overexpression suggests that angiogenesis-driven stromal remodeling contributes both to the radiographic appearance and to tumor aggressiveness. This mechanistic link explains our finding that patients with more than five spiculations faced a 2.15-fold increased mortality risk, highlighting the potential of imaging features as non-invasive biomarkers of tumor biology.

Furthermore, our quantitative imaging-pathology correlations align with known epidemiological trends. The observed 11.5-year age difference between malignant and benign cases (59.2 vs. 48.7 years) coincides with the peak incidence of stromal senescence, during which telomere attrition in fibroblasts promotes a protumorigenic microenvironment through the senescence-associated secretory phenotype (SASP). This age-related stromal remodeling likely underlies the higher prevalence of spiculated margins - a radiological surrogate for desmoplastic response - in older patients. Such mechanistic alignment supports the hypothesis that mammographic spiculations could serve as non-invasive biomarkers of stromal aging, potentially guiding the development of senolytic therapeutic strategies.

Finally, the combined use of mammography and ultrasonography demonstrated superior sensitivity, specificity, accuracy, and predictive values compared to either modality alone. Specifically, the combined approach yielded a sensitivity of 95.9%, specificity of 80.6%, and accuracy of 89.6%, all significantly higher than those of individual modalities. The high sensitivity indicates excellent ability to detect malignant lesions, which is crucial for early diagnosis and timely treatment. The moderate to high specificity reduces unnecessary biopsies by effectively ruling out benign lesions. Collectively, these results confirm that multimodal imaging offers robust diagnostic efficiency for breast cancer associated with structural distortions.

The PPV and NPV of the combined approach were 90.2% and 88.9%, respectively. A higher PPV indicates that when the combined model identifies a malignant lesion, there is a high probability that the lesion is truly malignant [27]. Conversely, the high NPV means that when the combined model excludes malignancy, the lesion is likely benign [28]. In clinical practice, these predictive values are critical for guiding the need for further diagnostic procedures and timely treatment decisions. Moreover, the AUC for the combined model was 0.91, significantly exceeding that of mammography (0.79) or ultrasonography (0.82) alone, highlighting the diagnostic advantage of integrating both modalities.

Subgroup analyses further demonstrated that the combined model maintained high sensitivity and moderate-to-high specificity across different age groups and menopausal statuses. Accuracy consistently ranged from 88.9% to 89.7%, reinforcing the effectiveness and potential generalizability of this approach in diverse clinical scenarios [29-31]. Clinically, our radiomic-molecular model (AUC=0.94) offers a promising pathway for personalized diagnostics. For example, lesions with spiculation complexity scores >2.5 and VEGF positivity (**Table 5**) could bypass intermediate BI-RADS 4A categorization, proceeding directly to biopsy. Conversely, low-risk radiomic profiles (probability <0.2) may justify short-term imaging follow-up, safely reducing unnecessary biopsies by 32% (**Table 6**).

The prognostic stratification revealed by this study has direct clinical implications. Patients classified as radiomic-molecular high-risk (5-year DFS of 62%) may benefit from intensified adjuvant therapy - consistent with evidence from the CREATE-X trial, which showed survival benefits from capecitabine in high-risk HER2-negative patients. In contrast, the excellent DFS in the low-risk group (94%) supports consideration of treatment de-escalation, in line with emerging trials aimed at minimizing overtreatment. Notably, the model maintained prognostic accuracy even in dense breasts, addressing a key diagnostic challenge: 75% of false negatives were observed in BI-RADS C/D density categories due to masking effects.

Despite robust findings, the study has notable limitations. First, its single-center retrospective design introduces selection bias, as it included only mammographically visible distortions - 75% of false negatives occurred in dense breast tissue, a gap that MRI radiomics could address. Second, radiomic features relied on vendor-specific protocols (GE LOGIQ9/ Fuji FDR-3000), potentially limiting cross-platform reproducibility. Third, semi-quantitative VEGF

immunohistochemistry (30% positivity threshold) and serum TGF-β1 may not fully reflect tumor biology. Finally, the model's prognostic utility in therapeutic contexts (e.g., VEGF-targeted therapies) remains unvalidated.

Future research should prioritize multicenter trials with standardized protocols (following IBSI guidelines), incorporate MRI to improve dense breast diagnostics, and validate long-term outcomes (beyond 5 years, especially in hormone receptor-positive subtypes).

Mammography and ultrasonography offer non-invasive, real-time evaluation of lesion morphology (e.g., spiculation, microcalcifications) and vascularity, enabling longitudinal monitoring without biopsy. However, they face limitations: operator dependence (interobserver kappa =0.78 for ultrasound), reduced specificity in dense breasts (BI-RADS C/D), and inability to assess molecular subtypes. By contrast, pathology remains essential for definitive diagnosis, precise molecular profiling (e.g., VEGF, TGF-β1), and stromal invasion grading.

This study confirms that integrating mammographic-ultrasonic features (e.g., spiculation complexity, hypervascularity) improves diagnostic accuracy for breast distortions, reducing unnecessary biopsies by 32% while stratifying prognosis (5-year DFS: 62% vs. 94% for high- vs. low-risk groups). The radiomic-pathologic model linking imaging phenotypes to VEGF advances precision diagnostics beyond traditional BI-RADS. Future efforts should focus on standardized radiomic pipelines, AI-assisted fusion of mammographic and ultrasonic features, and multicenter validation - particularly for BI-RADS 4 lesions and dense breast populations.

Acknowledgements

This study was supported by the Health Department of Hebei Province (No. 20201436).

Disclosure of conflict of interest

None.

Address correspondence to: Guang Yang, Department of Radiology, Fourth Hospital of Hebei Medical University, Shijiangzhuang 050011, Hebei, China. E-mail: 47200655@hebmu.edu.cn

References

[1] Barzaman K, Karami J, Zarei Z, Hosseinzadeh A, Kazemi MH, Moradi-Kalbolandi S, Safari E and Farahmand L. Breast cancer: biology, biomarkers, and treatments. Int Immunopharmacol 2020; 84: 106535.

[2] Monticciolo DL, Newell MS, Moy L, Lee CS and Destounis SV. Breast cancer screening for women at higher-than-average risk: updated recommendations from the ACR. J Am Coll Radiol 2023; 20: 902-914.

[3] Al-Karawi D, Al-Zaidi S, Helael KA, Obeidat N, Mouhsen AM, Ajam T, Alshalabi BA, Salman M and Ahmed MH. A review of artificial intelligence in breast imaging. Tomography 2024; 10: 705-726.

[4] Wilkinson L and Gathani T. Understanding breast cancer as a global health concern. Br J Radiol 2022; 95: 20211033.

[5] Katsura C, Ogunmwonyi I, Kankam HK and Saha S. Breast cancer: presentation, investigation and management. Br J Hosp Med (Lond) 2022; 83: 1-7.

[6] Zhang YN, Xia KR, Li CY, Wei BL and Zhang B. Review of breast cancer pathologigcal image processing. Biomed Res Int 2021; 2021: 1994764.

[7] Sechopoulos I, Teuwen J and Mann R. Artificial intelligence for breast cancer detection in mammography and digital breast tomosynthesis: state of the art. Semin Cancer Biol 2021; 72: 214-225.

[8] Coffey K and Jochelson MS. Contrast-enhanced mammography in breast cancer screening. Eur J Radiol 2022; 156: 110513.

[9] Obeagu EI and Obeagu GU. Breast cancer: a review of risk factors and diagnosis. Medicine (Baltimore) 2024; 103: e36905.

[10] Uematsu T. Rethinking screening mammography in Japan: next-generation breast cancer screening through breast awareness and supplemental ultrasonography. Breast Cancer 2024; 31: 24-30.

[11] Jiang K, Ma C, Yang Y, McKevitt E, Pao JS, Warburton R, Dingee C, Bremang JN, Deban M and Bazzarelli A. Axillary ultrasonography for early-stage invasive breast cancer. Am J Surg 2024; 231: 86-90.

[12] Erdinç Gündüz N, Dilek B, Şahin E, Ellidokuz H and Akalın E. Diagnostic contribution of ultrasonography in breast cancer-related lymphedema. Lymphat Res Biol 2021; 19: 517-523.

[13] Bodewes FTH, van Asselt AA, Dorrius MD, Greuter MJW and de Bock GH. Mammographic breast density and the risk of breast cancer: a systematic review and meta-analysis. Breast 2022; 66: 62-68.

[14] Resch D, Lo Gullo R, Teuwen J, Semturs F, Hummel J, Resch A and Pinker K. AI-enhanced mammography with digital breast tomosynthesis for breast cancer detection: clinical value and comparison with human performance. Radiol Imaging Cancer 2024; 6: e230149.
[15] Díaz O, Rodríguez-Ruíz A and Sechopoulos I. Artificial intelligence for breast cancer detection: technology, challenges, and prospects. Eur J Radiol 2024; 175: 111457.
[16] Henderson JT, Webber EM, Weyrich MS, Miller M and Melnikow J. Screening for breast cancer: evidence report and systematic review for the US preventive services task force. JAMA 2024; 331: 1931-1946.
[17] Wang Q, Lin Y, Ding C, Guan W, Zhang X, Jia J, Zhou W, Liu Z and Bai G. Multi-modality radiomics model predicts axillary lymph node metastasis of breast cancer using MRI and mammography. Eur Radiol 2024; 34: 6121-6131.
[18] Price MD, Mali ME, Dedey F, Dzefi-Tettey K, Li Y, Almeida C, Brownson KE, Price RR and Sutherland EK. Mammography and breast ultrasonography services in ghana, availability, and geographic access. JCO Glob Oncol 2024; 10: e2400218.
[19] Hernström V, Josefsson V, Sartor H, Schmidt D, Larsson AM, Hofvind S, Andersson I, Rosso A, Hagberg O and Lång K. Screening performance and characteristics of breast cancer detected in the Mammography Screening with Artificial Intelligence trial (MASAI): a randomised, controlled, parallel-group, non-inferiority, single-blinded, screening accuracy study. Lancet Digit Health 2025; 7: e175-e183.
[20] Chung WS, Wan TTH, Shiu YT and Shi HY. Cost-effectiveness analysis of digital breast tomosynthesis and mammography in breast cancer screening: a markov modeling study. J Epidemiol Glob Health 2024; 14: 933-946.
[21] Kataoka M and Uematsu T. AI systems for mammography with digital breast tomosynthesis: expectations and challenges. Radiol Imaging Cancer 2024; 6: e240171.
[22] Zuley ML, Bandos AI, Duffy SW, Logue D, Bhargava R, McAuliffe PF, Brufsky AM and Nishikawa RM. Breast cancer screening interval: effect on rate of late-stage disease at diagnosis and overall survival. J Clin Oncol 2024; 42: 3837-3846.
[23] Song H, Tran TXM, Kim S and Park B. Risk factors and mortality among women with interval breast cancer vs screen-detected breast cancer. JAMA Netw Open 2024; 7: e2411927.
[24] Bitencourt A, Daimiel Naranjo I, Lo Gullo R, Rossi Saccarelli C and Pinker K. AI-enhanced breast imaging: where are we and where are we heading? Eur J Radiol 2021; 142: 109882.
[25] Lo Gullo R, Brunekreef J, Marcus E, Han LK, Eskreis-Winkler S, Thakur SB, Mann R, Groot Lipman K, Teuwen J and Pinker K. AI applications to breast MRI: today and tomorrow. J Magn Reson Imaging 2024; 60: 2290-2308.
[26] Glechner A, Wagner G, Mitus JW, Teufer B, Klerings I, Böck N, Grillich L, Berzaczy D, Helbich TH and Gartlehner G. Mammography in combination with breast ultrasonography versus mammography for breast cancer screening in women at average risk. Cochrane Database Syst Rev 2023; 3: Cd009632.
[27] Bernini M, Spolveri F, Tofani L, De Benedetto D, Bicchierai G, Bellini C, Morrone D, Nori Cucchiari J, Bianchi S, Livi L, Orzalesi L and Meattini I. B3 breast lesions: positive predictive value and follow-up on a large single-institution series. J Surg Res 2024; 299: 366-373.
[28] Lauritzen AD, Lillholm M, Lynge E, Nielsen M, Karssemeijer N and Vejborg I. Early indicators of the impact of using AI in mammography screening for breast cancer. Radiology 2024; 311: e232479.
[29] Balkenende L, Teuwen J and Mann RM. Application of deep learning in breast cancer imaging. Semin Nucl Med 2022; 52: 584-596.
[30] Rahman WT and Helvie MA. Breast cancer screening in average and high-risk women. Best Pract Res Clin Obstet Gynaecol 2022; 83: 3-14.
[31] Wekking D, Porcu M, De Silva P, Saba L, Scartozzi M and Solinas C. Breast MRI: clinical indications, recommendations, and future applications in breast cancer diagnosis. Curr Oncol Rep 2023; 25: 257-267.